Supporting Information for

Combined experimental, theoretical and molecular simulation approach for the description of the fluid phase behavior of hydrocarbon mixtures within shale rocks

Carmelo Herdes[b], Camille Petit[a], Andres Mejía[c] and Erich A. Müller[a,*]

[a] Department of Chemical Engineering, Imperial College London, U.K.
[b] Department of Chemical Engineering, Bath University, U.K.
[c] Departamento de Ingeniería Química, Universidad de Concepción, Chile

* Author to whom correspondence should be addressed (e.muller@imperial.ac.uk)

S.1 Samples.

Four shale core samples were employed, referenced herein as A, B, C & D received in the laboratory in pristine state.

S.2. Characterization of Samples

S.2.1. Nitrogen isotherms

N_2 sorption isotherms are measured at 77 K using a 3Flex sorption analyzer (Micromeritics). Prior to the measurement, the samples are degassed overnight at 120 °C using a sample degas system (Micromeritics, VacPrep 061) and then in-situ for 5 hours at 120 °C down to 0.1 mmHg. The BET surface areas and the total volumes of pores (derived from the point at $P/P_0 = 0.97$) are calculated from the isotherms.

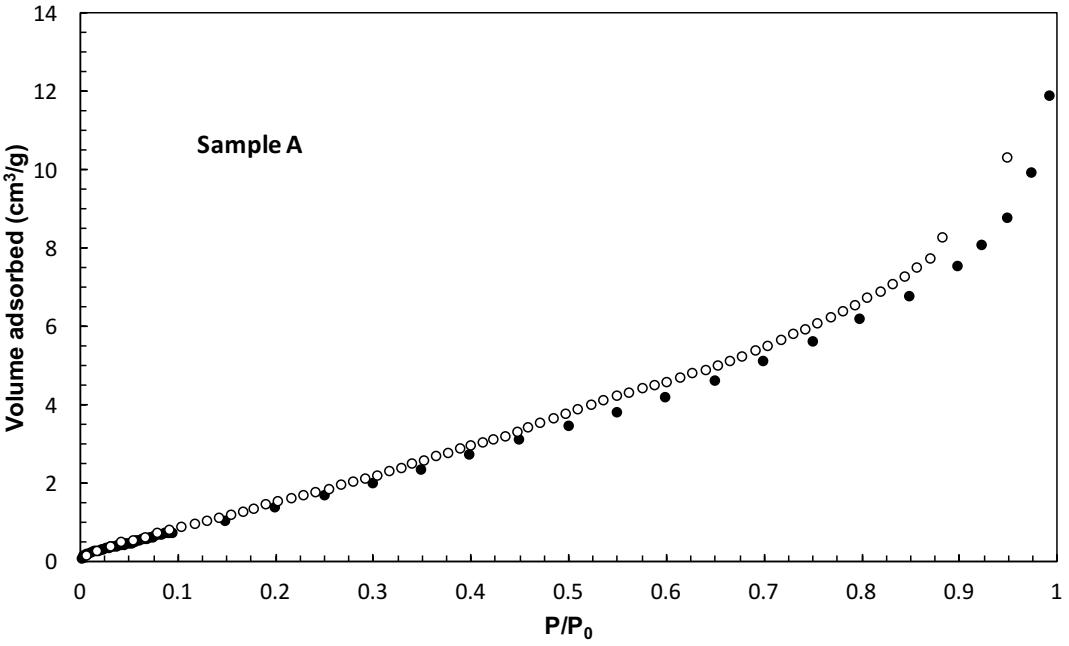

Figure S1 Nitrogen adsorption isotherms (77K) on Sample A. Solid symbols are adsorption, open symbols desorption.

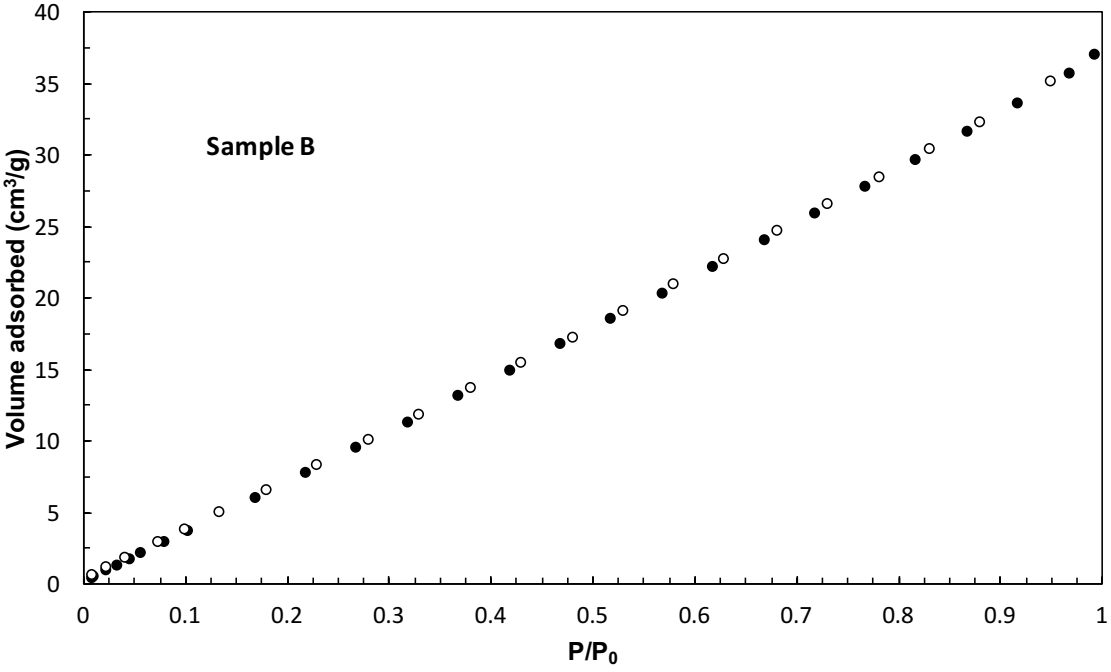

Figure S2 Nitrogen adsorption isotherms (77K) on Sample B. Solid symbols are adsorption, open symbols desorption.

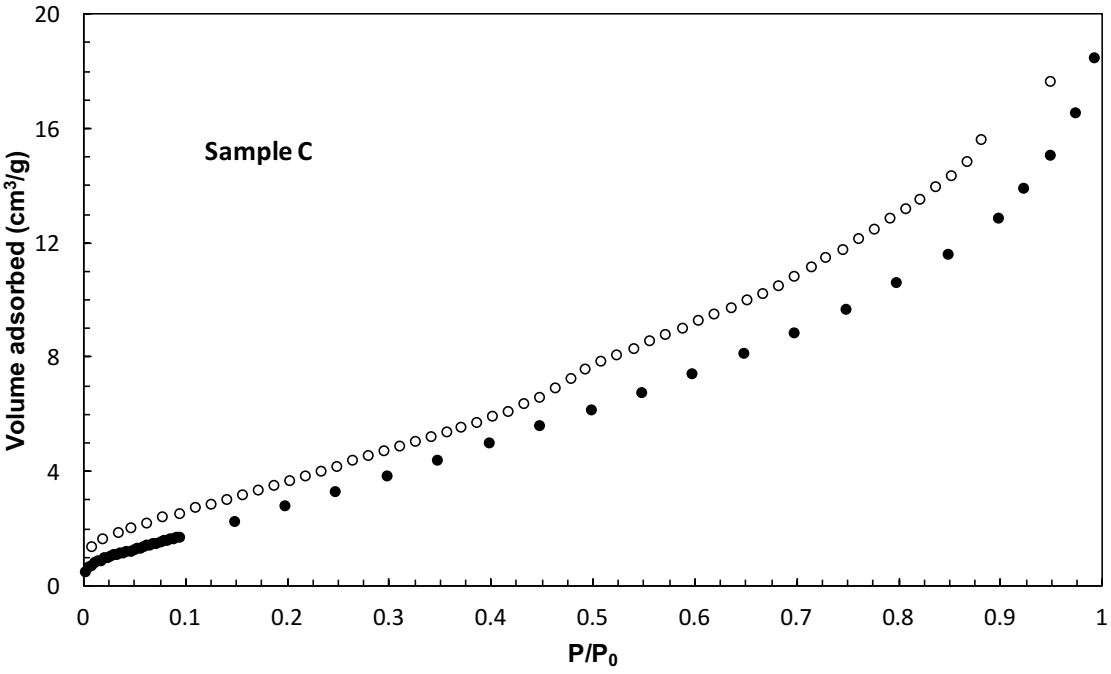

Figure S3 Nitrogen adsorption isotherms (77K) on Sample C. Solid symbols are adsorption, open symbols desorption.

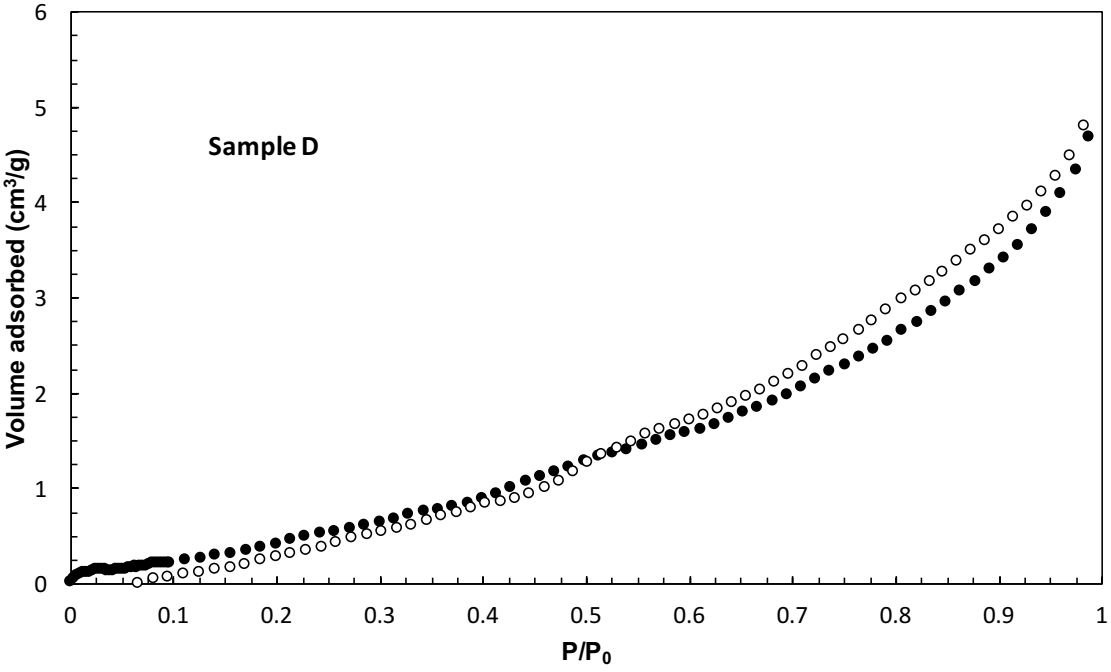

Figure S4 Nitrogen adsorption isotherms (77K) on Sample D. Solid symbols are adsorption, open symbols desorption.

S.2.2. Pore size distributions

The pore size distribution is obtained from these isotherms using standard density functional theory-based packages.

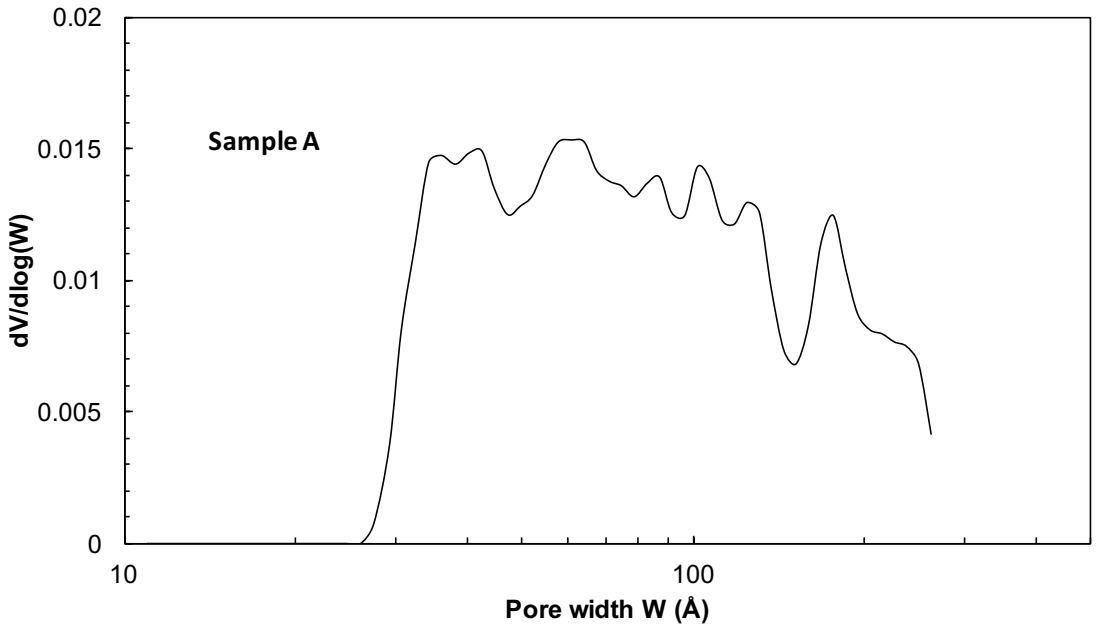

Figure S5 Pore size distributions of sample A estimated from a DFT analysis of the nitrogen adsorption isotherms.

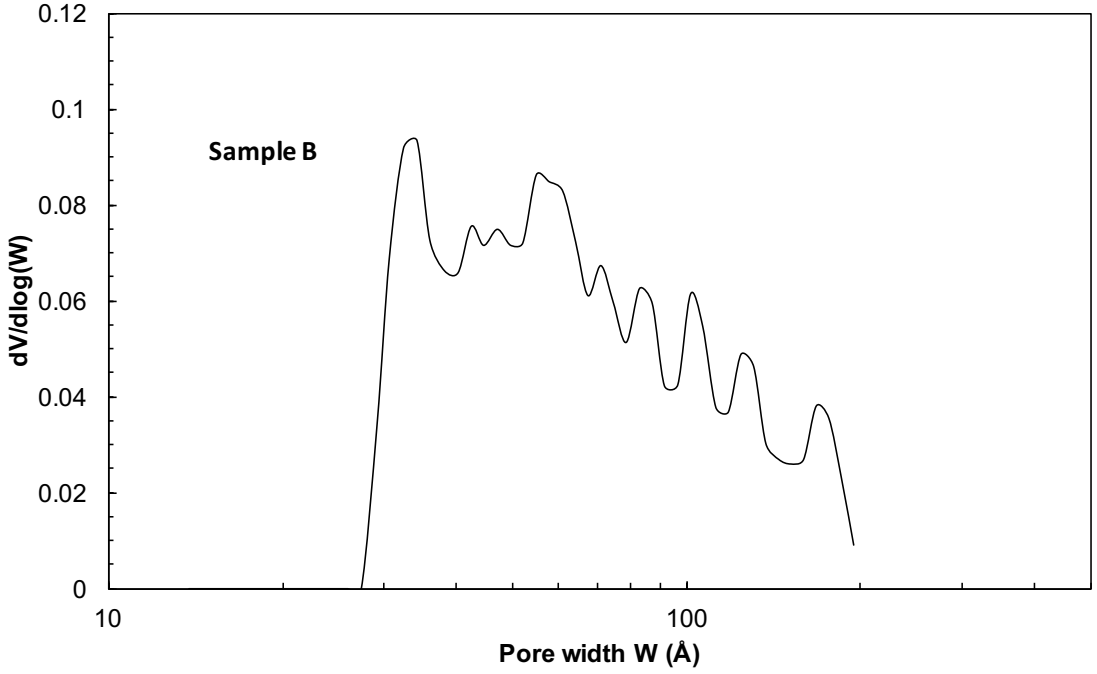

Figure S6 Pore size distributions of sample B estimated from a DFT analysis of the nitrogen adsorption isotherms.

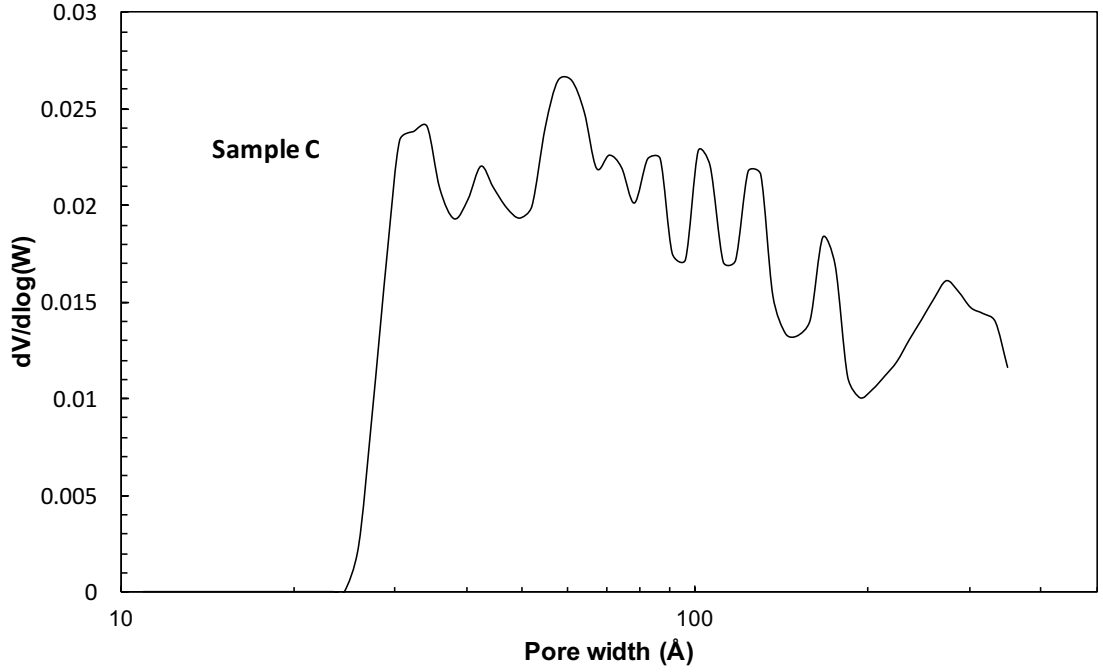

Figure S7 Pore size distributions of sample C estimated from a DFT analysis of the nitrogen adsorption isotherms.

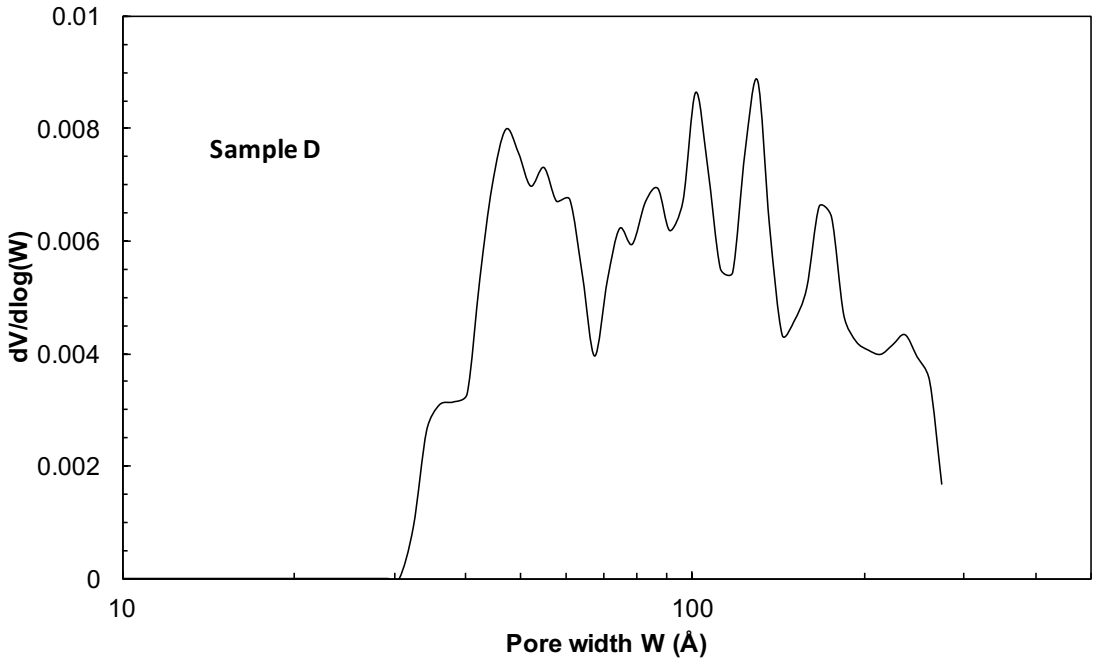

Figure S8 Pore size distributions of sample D estimated from a DFT analysis of the nitrogen adsorption isotherms.

S.2.3. Raw X-ray diffraction (XRD) spectra

Measurements were performed on a D4 Endeavor with radiation Cu-α1 (λ = 1.5406 Å) at 30 kV and 15 mA, divergence slit V20.

Prior to the measurement, the samples are dried overnight at 120 °C and then crushed and sieved at mesh 400.

Red symbols are calcium carbonate – $CaCo_3$, blue (or green) symbols are silicon oxide SiO_2

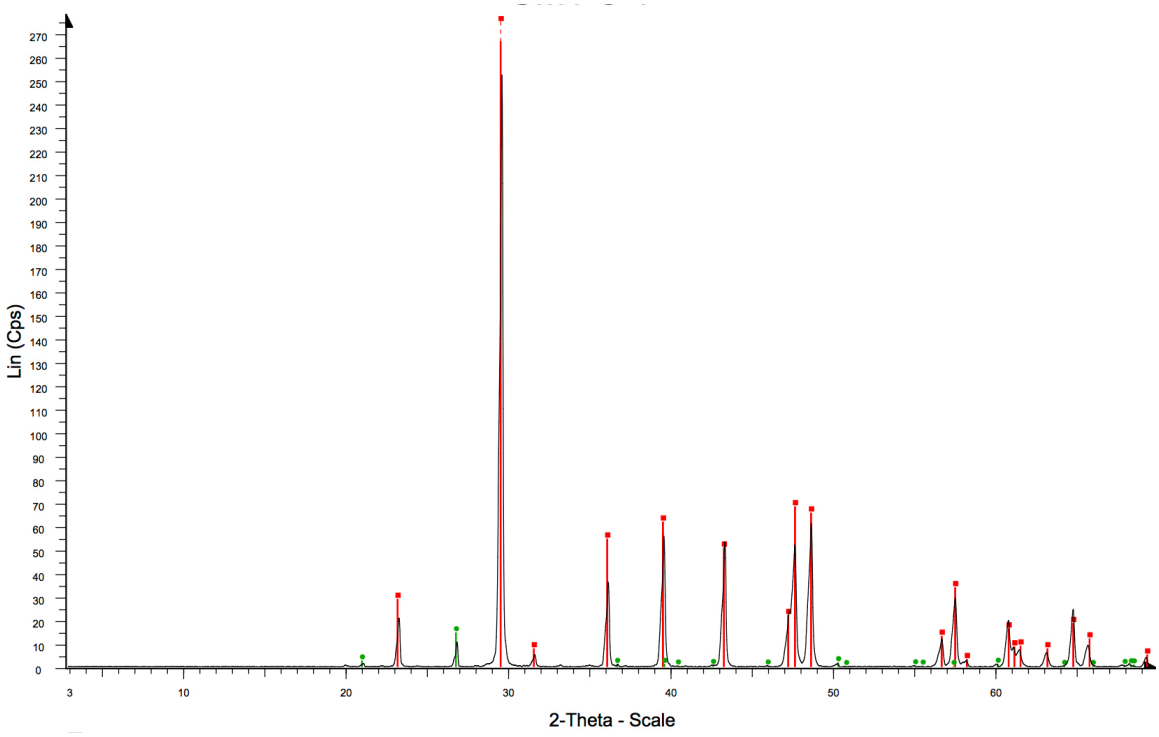

Figure S9 XRD of sample A

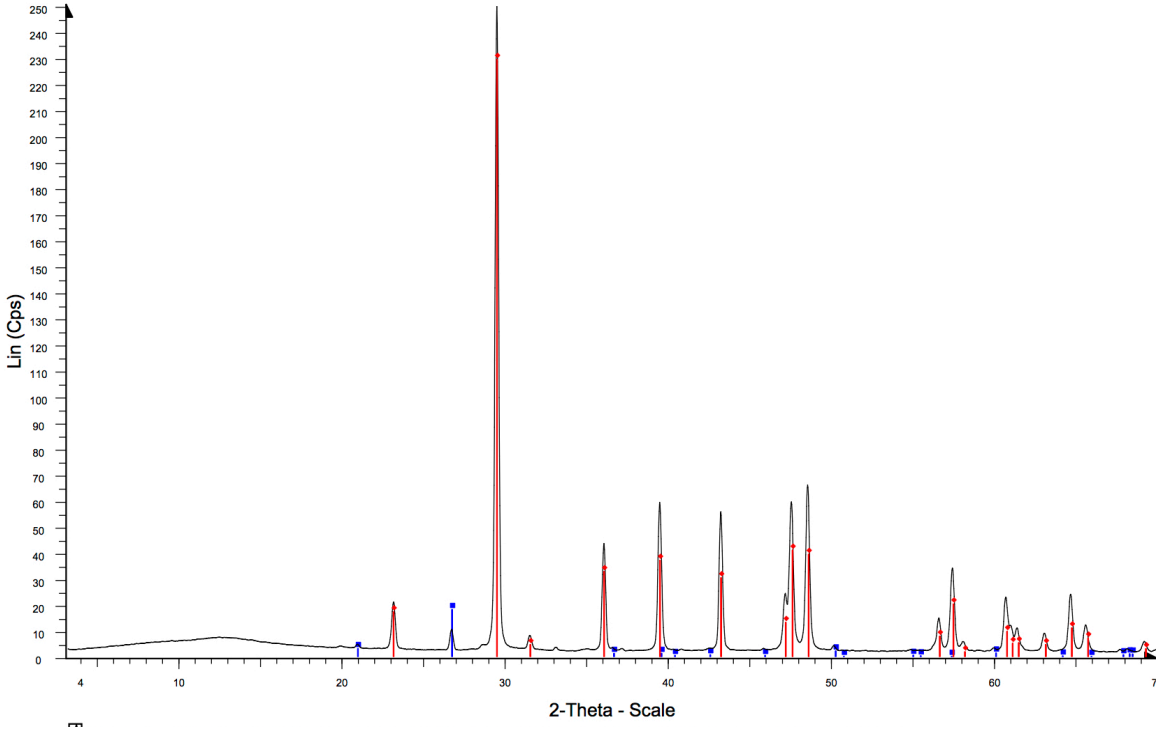

Figure S10 XRD of sample B

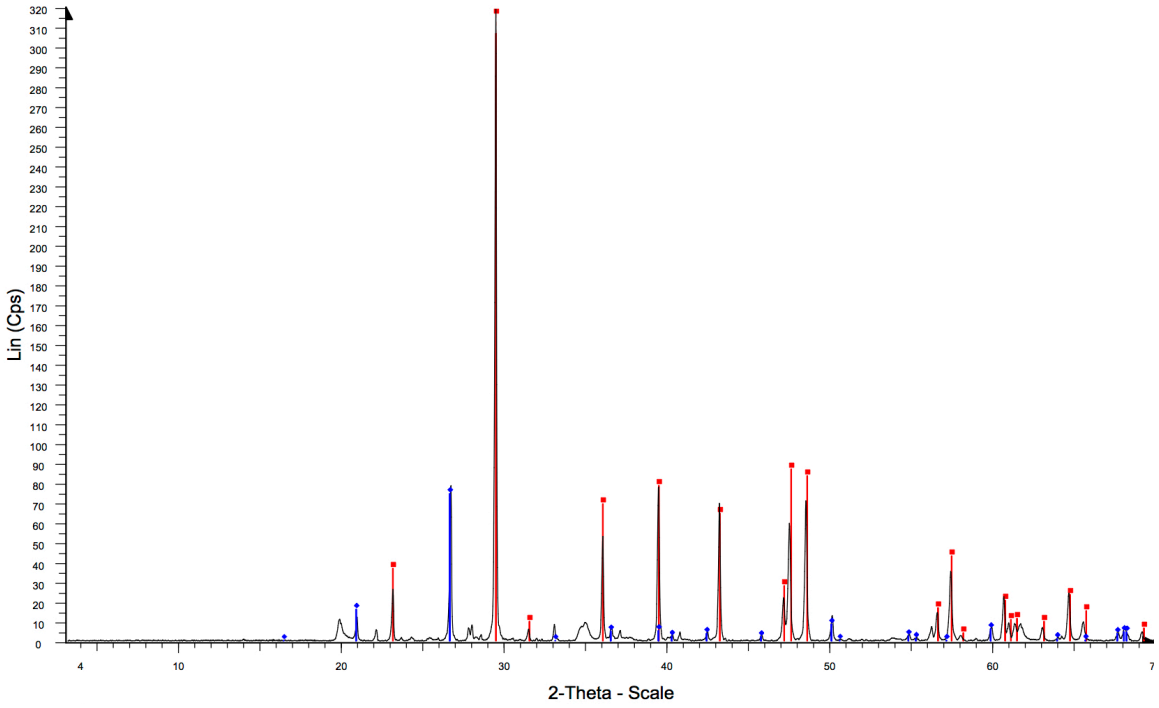

Figure S11 XRD of sample C

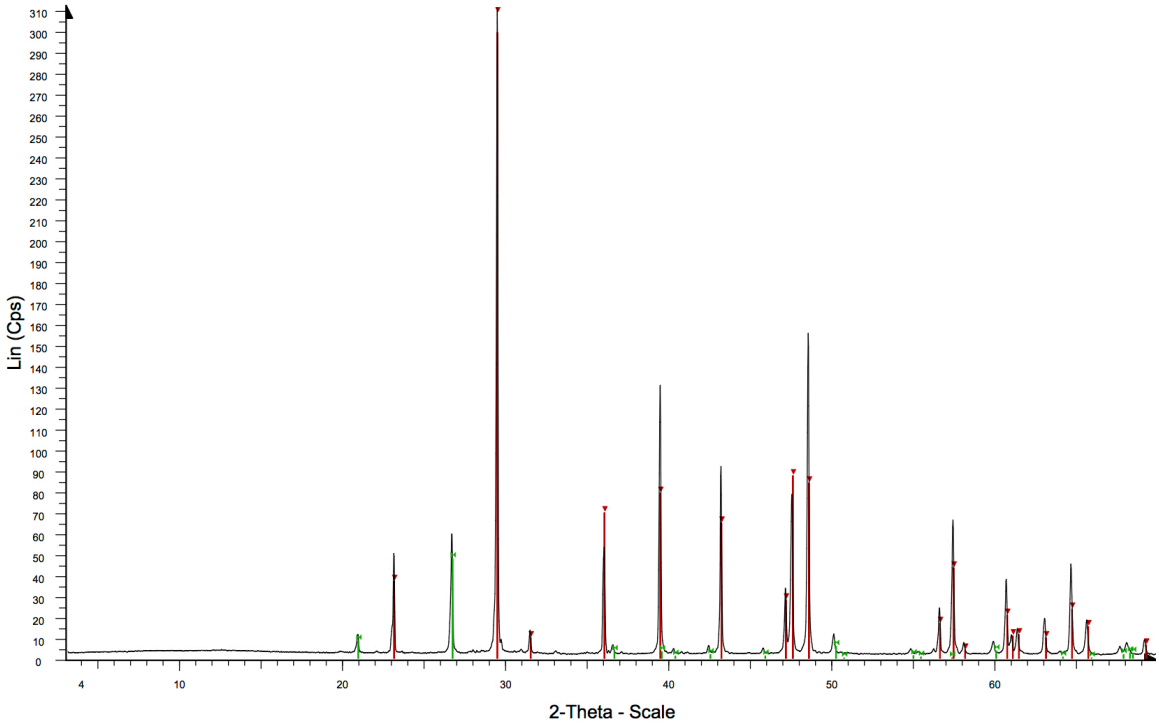

Figure S12 XRD of sample D

S.2.3.5 Thermogravimetric analysis

The thermal stability of the shale samples is evaluated using a Netzsch TG 209 F1 Libra thermogravimeter. The samples (about 10 and 20 mg) are placed in ceramic crucibles and heated in air from 25 °C to 900 °C at a heating rate of 10 °C/min. The total flow rate was 120 mL/min.

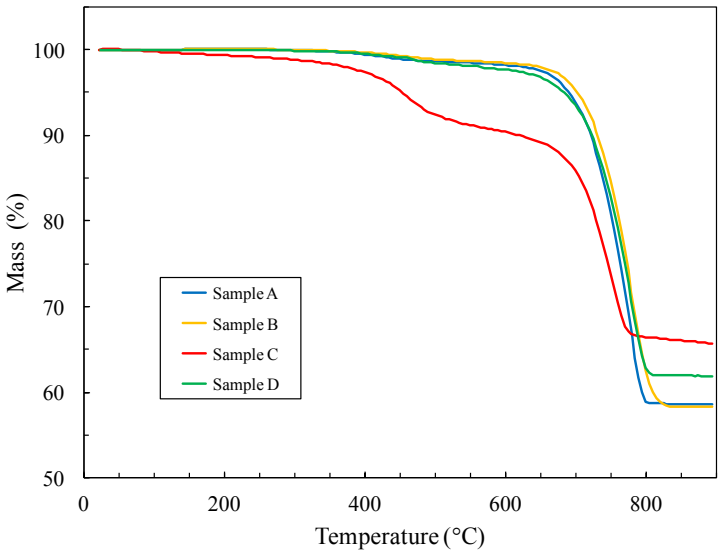

Figure S13 TGA curves

S.3 SEM images

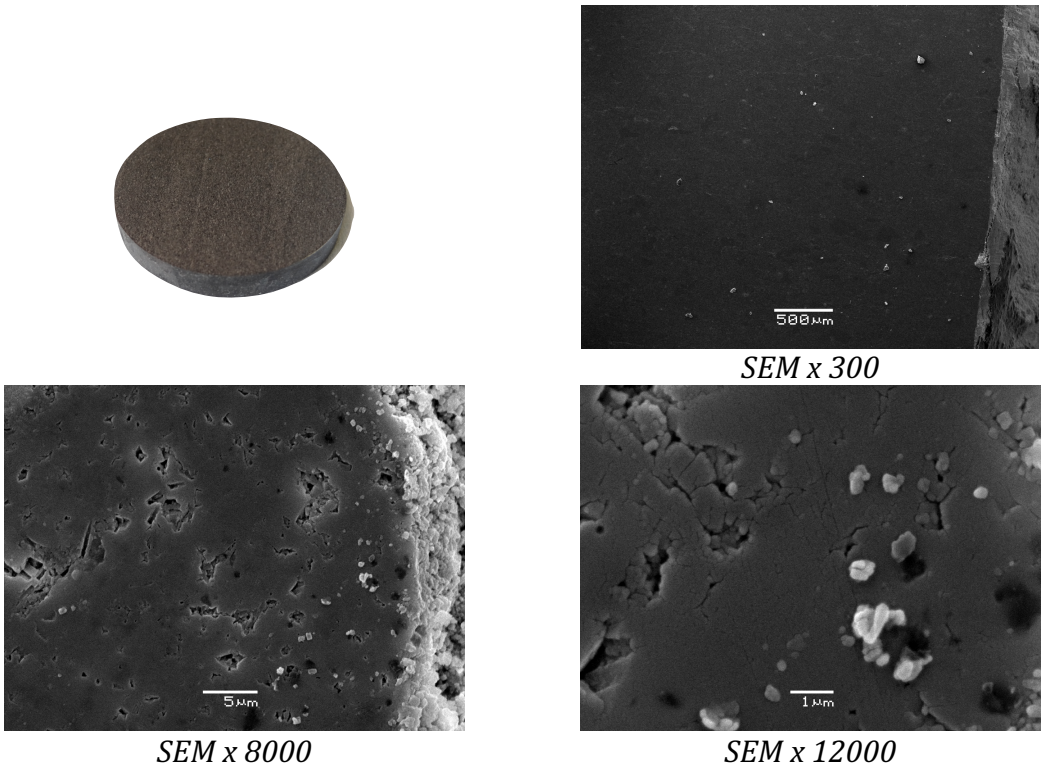

Figure S14 Photograph of the polished sample (upper left) and Scanning Electron Microscopy (SEM) images for sample A.

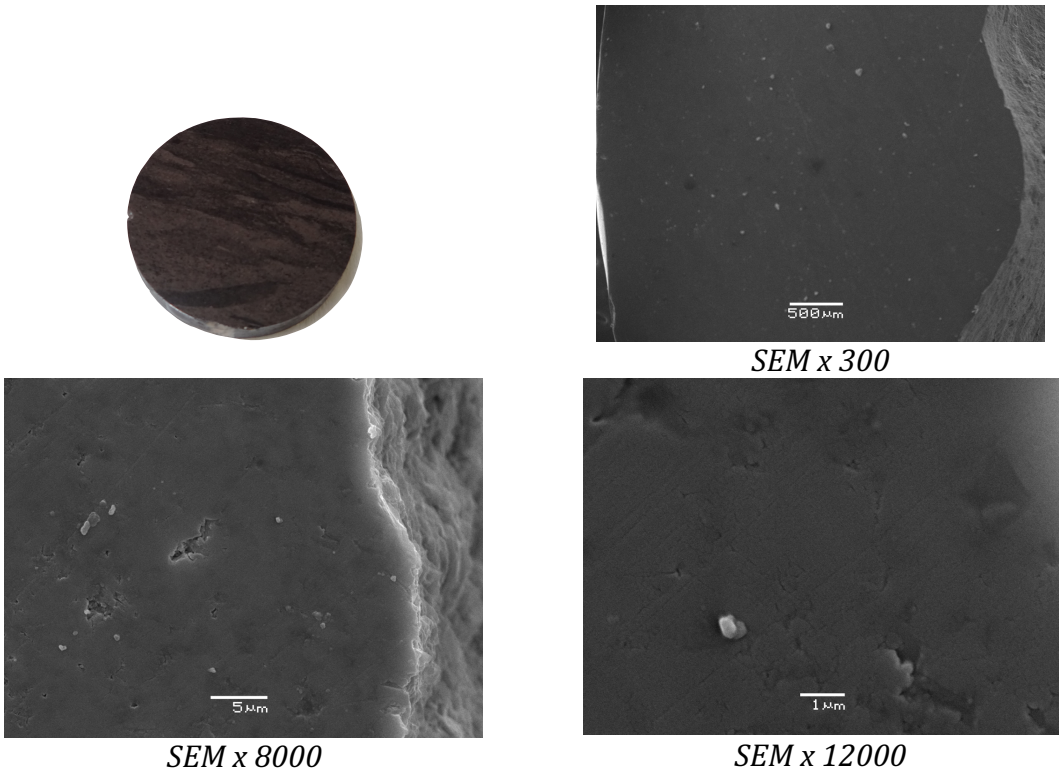

Figure S15 Photograph of the polished sample (upper left) and Scanning Electron Microscopy (SEM) images for sample B.

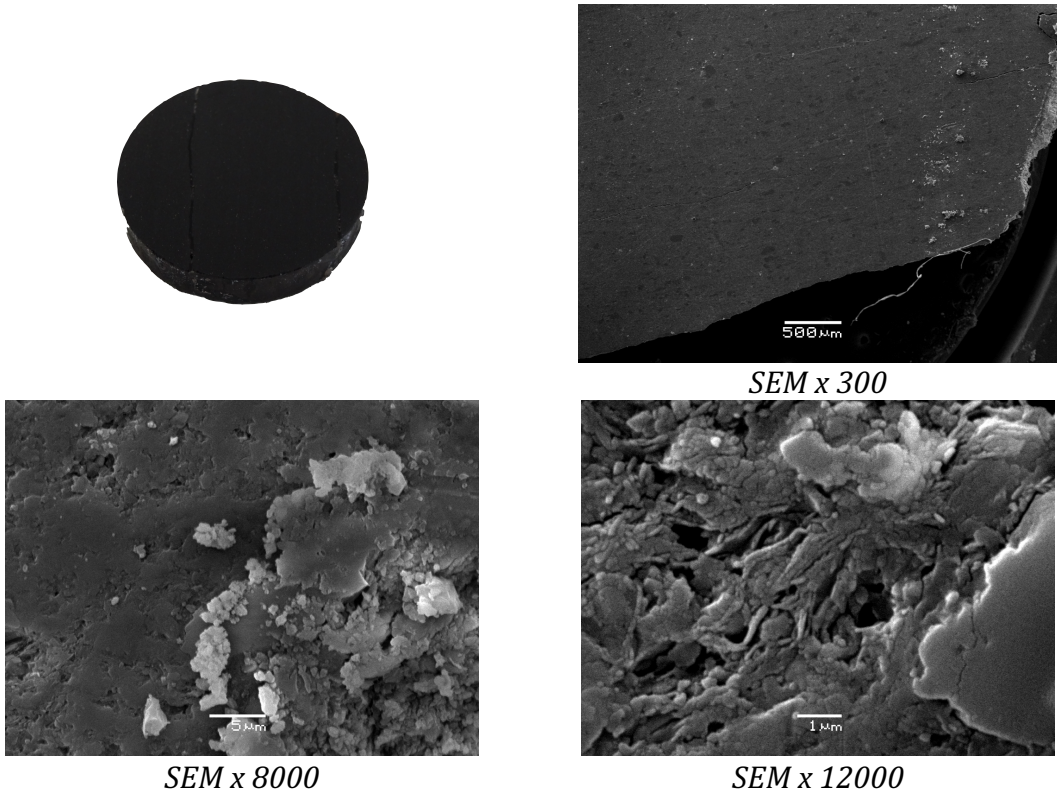

Figure S16 Photograph of the polished sample (upper left) and Scanning Electron Microscopy (SEM) images for sample C.

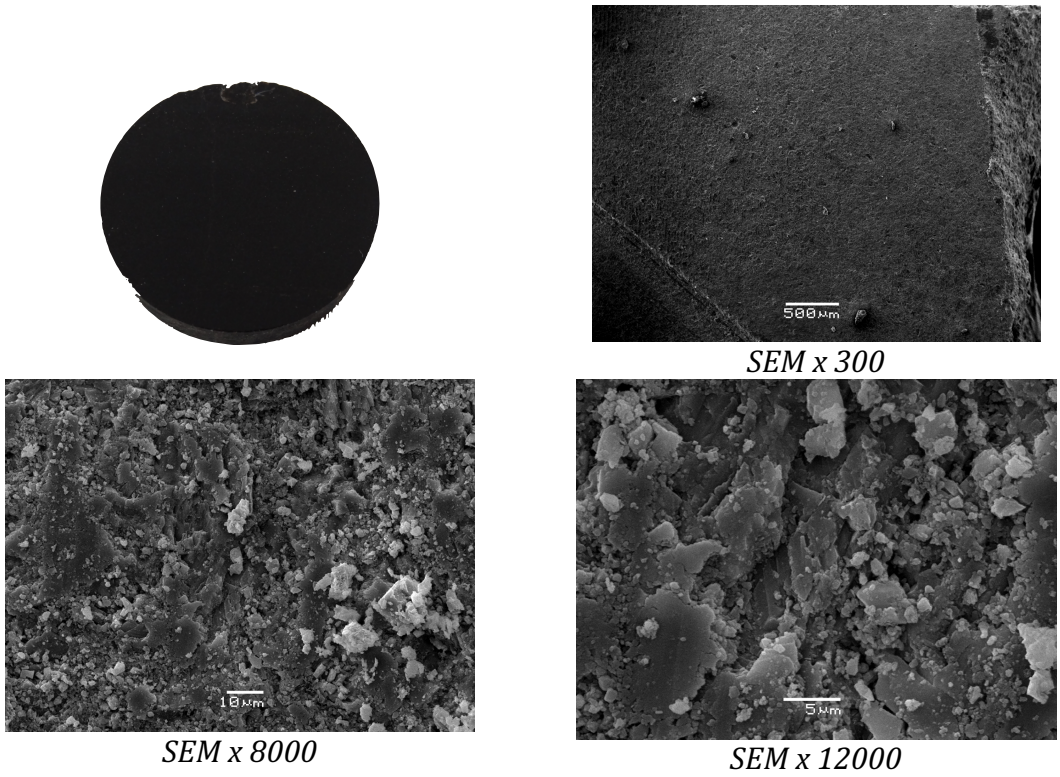

Figure S17 Photograph of the polished sample (upper left) and Scanning Electron Microscopy (SEM) images for sample D.

S4. Contact angle measurements

S.4.1 Experimental setup

A pendant drop tensiometer model IFT-10, manufactured by Temco Inc. (USA) is used in contact angle measurements. The pendant drop cell is a stainless steel cylindrical chamber (with an inner volume of ~ 42 cm^3), with two injection orifices one at the top and the other at the bottom of the chamber. On the top orifice, a stainless steel needle is placed for generating pendant drops, which are deposited in the solid surface. The bottom orifice is used to place the solid support and to connect to the high-pressure syringe pump (Teledyne Isco Pump. Model 100DM, USA), which is used to compress the inert gas from a commercial ultra-high purity cylinder. The chamber is equipped with appropriately sealed borosilicate glass windows, which allow visualization of the inner space during operation.

The experimental procedure for determining contact angles is as follows. The solid surface is placed in the sample support in the pendant drop chamber. The chamber is closed and it is heated to the desired experimental temperature, and then it is slightly pressurized with the inert gas. After degasification in an ultrasonic bath, the liquid is pumped through a stainless steel tube to the needle tip. The pump is a positive displacement ELDEX HP Series Model B-100-S-2 CE (USA). Initially, a small portion of the pure liquid is pumped into the chamber in order to saturate the gas that fills the cell. Then, the cell is pressurized to the desired experimental pressure and a liquid drop is deposited in the solid surface. The pressure in the IFT cell is maintained constant to within ± 0.10 kPa by means of the high-pressure syringe pump. Once the drop is formed and the desired experimental temperature and pressure are reached, it is necessary to wait, approximately, 1 to 5 minutes until the drop reaches an equilibrium state. After this equilibration step, the contact angles are recorded (at least during 30 min) in order to check the stability of its geometry. Once the shape and volume of the drop are deemed constant, the different contact angles on the right and left side of the drop are recorded. The reported contacts angle will be an average over, al least, 10 measurements on different positions of the solid sample. The precision of contact angle measurements ± 0.1°. The camera magnification, i.e. the relation between dimensions and pixels, is calibrated by reproducing the value of the diameter of a needle of known dimensions, at fixed light intensity and camera operation parameters (position and zoom). Finally, we note that the impeccable cleaning of the chamber plays a key role in the accuracy of the pendant drop technique, as minuscule impurities may strongly affect tension measurements. Consequently, appropriate precautions were taken to this effect.

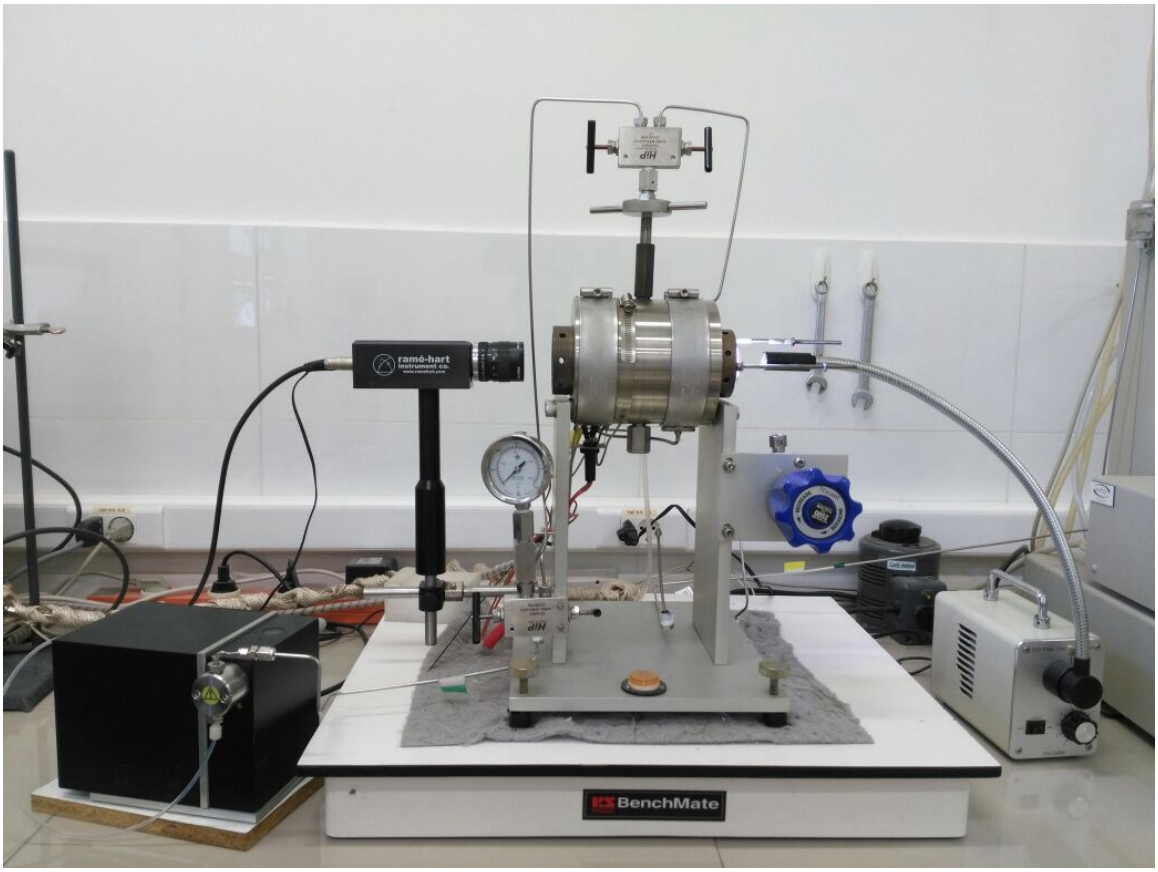

Figure S18. Pendant drop tensiometer used for contact angle measurements. Equipment is set up at the Cohesion lab, Depatment of Chemical Engineering, Concepción (care of Prof. Andrés Mejía). Range of *T* is from ambient to 150 °C and *P* from ambient to 62 MPa (9000 psi).

Figure S19 shows typical observations from the view window of the cell. The results are qualitatively similar for all the rock samples studied. Decane and CO_2 both exhibit complete wetting of the surface and contact angles must be measured as described in the previous section. Water exhibits only partial wetting and the contact angle measurement is done without the need of the injection needle.

Figure S19. View of the experimental cell for the case of the three fluids considered. The results for all solids is qualitatively similar.

S.4.2 Raw data

Using the polished samples, contact angles have been measured as a function of temperature and pressure for the four samples.

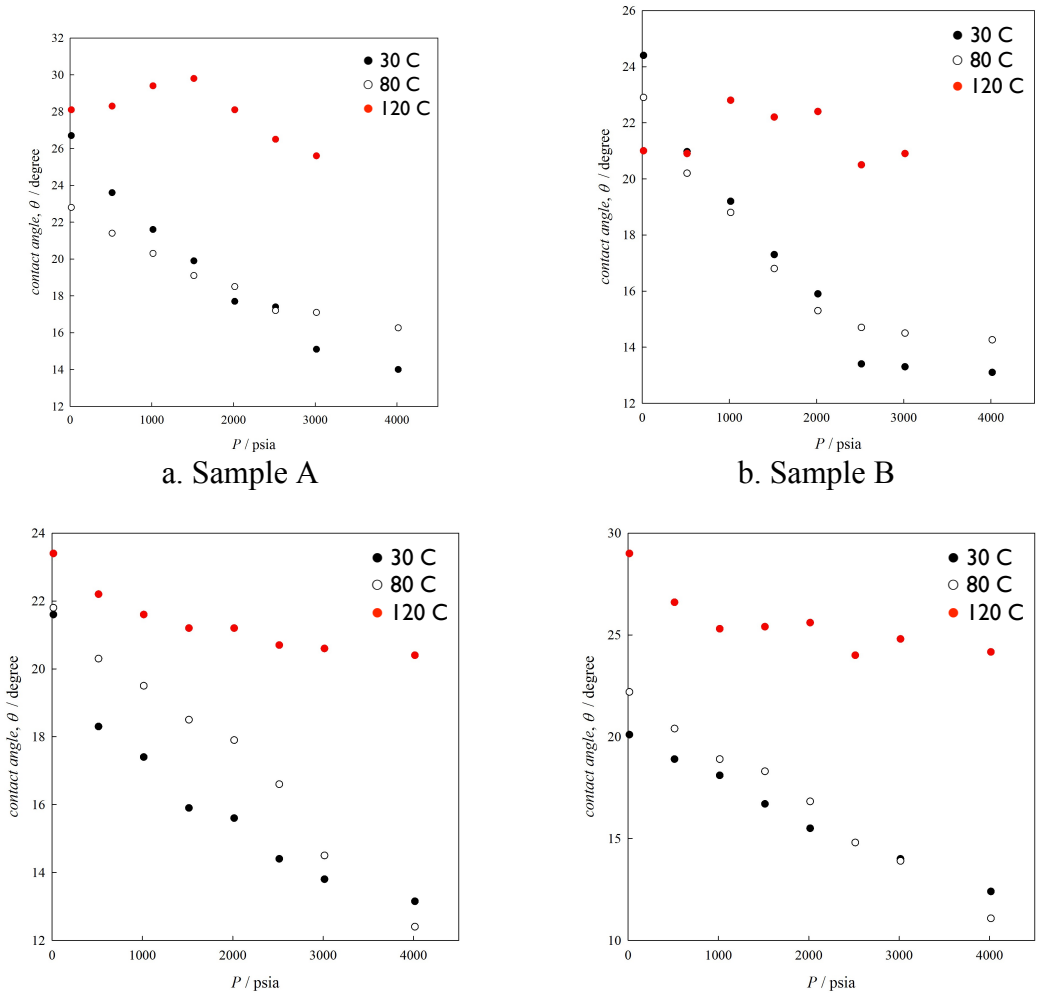

a. Sample A b. Sample B

c. Sample C d. Sample D

Figure S20. Experimental contact angles of decane over samples as a function of temperature and pressure.

The curves show a monotonous decrease of the contact angles as the pressure is increased. This is a somehow expected result, which is related to the change in thermophysical properties of the fluid rather than any particular effect of the surface-fluid interaction. Comparison with table 2 indicates that, as expected, the polishing of the surface has a profound effect on the results. This is a known complication of contact angle measurements[1] and is something that must be borne in mind when analyzing the results.

[1] D.Y. Kwok, A.W. Neumann (1999). Contact angle measurement and contact angle interpretation. *Advances in Colloid and Interface Science*, *81*(3), 167–249.

Table S1. Contact angles of decane over polished samples at 30 ^{o}C

T / C	psig	psia	Sample A	Sample B	Sample C	Sample D
30	0	14.69	26.70	24.40	21.60	20.10
30	500	514.69	23.60	20.97	18.30	18.90
30	1000	1014.69	21.60	19.20	17.40	18.10
30	1500	1514.69	19.90	17.30	15.90	16.70
30	2000	2014.69	17.70	15.90	15.60	15.50
30	2500	2514.69	17.40	13.40	14.40	14.80
30	3000	3014.69	15.10	13.30	13.80	14.00
30	4000	4014.69	14.00	13.10	13.15	12.40

Table S2. Contact angles of decane over polished samples at 80 ^{o}C

T / C	psig	psia	Sample A	Sample B	Sample C	Sample D
80	0	14.69	22.80	22.90	21.80	22.20
80	500	514.69	21.40	20.20	20.30	20.40
80	1000	1014.69	20.30	18.80	19.50	18.90
80	1500	1514.69	19.10	16.80	18.50	18.30
80	2000	2014.69	18.50	15.30	17.90	16.82
80	2500	2514.69	17.20	14.70	16.60	14.80
80	3000	3014.69	17.10	14.50	14.50	13.90
80	4000	4014.69	16.26	14.26	12.40	11.08

Table S3. Contact angles of decane over polished samples at 120 ^{o}C

T / C	psig	psia	Sample A	Sample B	Sample C	Sample D
120	0	14.69	28.1	21.0	23.4	29.0
120	500	514.69	28.3	20.9	22.2	26.6
120	1000	1014.69	29.4	22.8	21.6	25.3
120	1500	1514.69	29.8	22.2	21.2	25.4
120	2000	2014.69	28.1	22.4	21.2	25.6
120	2500	2514.69	26.5	20.5	20.7	24.0
120	3000	3014.69	25.6	20.9	20.6	24.8

In addition to n-decane,. water and CO_2 have been used to measure the contact angles over the samples. Table S5 summarizes the main results.

Table S4. Contact angles of water and CO_2 over polished samples

Sample	Water 30°C and 14.59 psia	CO_2 21°C and 850 psia
A	44.2	30.2
B	43.8	29.1
C	32.3	35.9
D	52.4	31.1

At higher temperatures CO_2 approaches its critical point and it is not possible to measure solid-fluid contact angles.

S.4.3 Fluid solid interactions for water

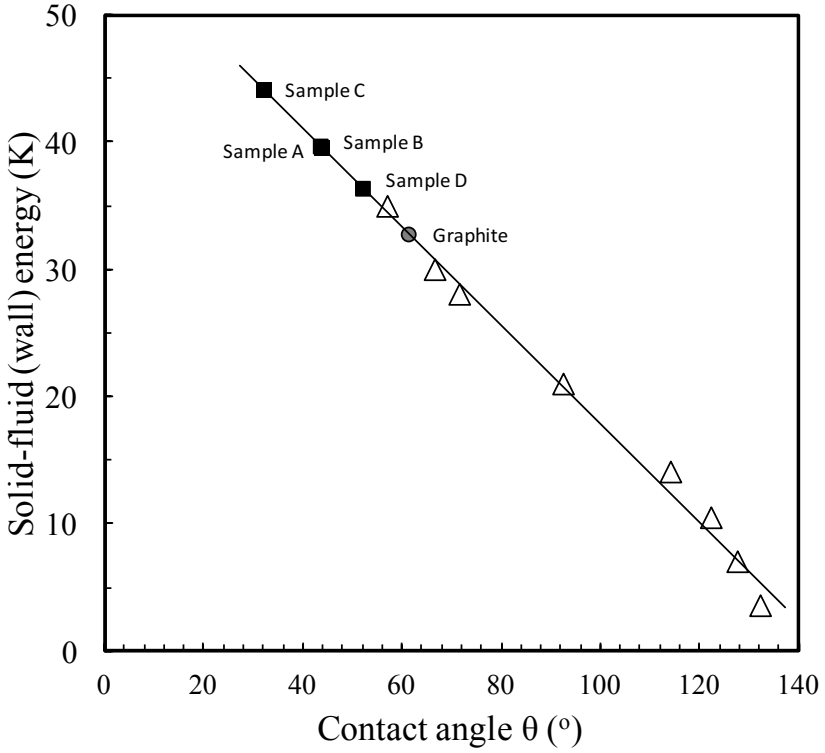

Figure S21. Contact angle θ (°) as a function of the solid-fluid (wall) interaction energy for water (right) at 30 °C and 0.1 MPa. Fluids are coarse-grained model with fluid-fluid energies given in Table 3. The solid-fluid energy of the surface (wall energy) is varied. Contact angles calculated from simulations and shown as open triangles. Grey circle corresponds to a graphite surface energy. Solid squares are the experimental results on real surfaces. Solid line is a best fit trendline.

S5. Fluid-fluid interactions

The parameters of the coarse-grained potentials are obtained by mapping the SAFT-γ-Mie equation of state to the vapor-liquid properties of the pure fluids in question. While one could perform a best-fit of several points (e.g. in the saturated liquid region and/or the vapor pressure curve), a short-cut method as described in Mejía et al.[1] is employed herein. The Mie potential can be expressed in a conformal manner in terms of three parameters

that relate to a length scale, σ, an energy scale, ε, and the range or functional form of the potential, λ, while the non-sphericity or elongation of a molecule can be appropriately described by the chain length, *m*. For a given chain length, Mejia el al provide correlations to scale the SAFT equation of state in terms of three experimental parameters: the acentric factor, the critical temperature, and the saturated liquid density at a reduced temperature of 0.7. The molecular nature of the equation of state is exploited to make a direct link between the macroscopic thermodynamic parameters used to characterize the equation of state and the parameters of the underlying Mie potential, hence the parameters obtained from the fitting of the equation of state can be used directly in the molecular simulation of the fluid.

Table S5 provides the data employed for the fitting of the new parameters introduced in this manuscript. Other sources of parameters are given in table 3 of the main manuscript.

Table S5. Experimental data[2] used to parametrize the SAFT force fields and the resulting force field parameters.

	Experimental (input) data			*SAFT force field parameters*			
Component	T_c *(K)*	ω	$\rho_L\|_{0.7}$ (mol/m^3)	*m*	σ *(nm)*	ε/k_B *(K)*	λ
methane	190.56	0.0114	24183	1	0.37523	170.75	16.39
pentane	469.7	0.251	8167.9	2	0.42477	317.50	16.06
n-decane	617.7	0.488	4336. 5	3	0.45841	415.19	20.92
naphthalene	748.4	0.302	6475.5	2	0.46228	557.75	19.50
carbon dioxide	304.13	0.224	26828	2	0.28485	194.94	14.65

[1] Mejía, A.; Herdes, C.; Müller, E. A. "Force Fields for Coarse-Grained Molecular Simulations From a Corresponding States Correlation." *Ind. Eng. Chem. Res* **2014**, *53*, 4131–41.

[2] E.W. Lemmon, M.O. McLinden, D.G. Friend, Thermophysical properties of fluid systems, in: P.J. Linstrom, W.G. Mallard (Eds.), NIST Chemistry WebBook, NIST Standard Reference Database Number 69, National Institute of Standards and Technology, Gaithersburg, MD 20899, 2015, ⟨http://webbook.nist.gov⟩ (retrieved April 4, 2018).